

Investigation of Safety in Human-Robot-Interaction for a Series Elastic, Tendon-Driven Robot Arm

Thomas Lens and Oskar von Stryk

Abstract—This paper presents the design of the lightweight BioRob manipulator with spring-loaded tendon-driven actuation developed for safe physical human-robot interaction. The safety of the manipulator is analyzed by an analytical worst-case estimation of impact and clamping forces in the absence of collision detection. As intrinsic joint compliance can pose a threat by storing energy, a safety evaluation method is proposed taking the potential energy stored in the elastic actuation into account. The evaluation shows that the robot arm design constrains the worst case clamping forces to only 25 N, while being able to handle loads up to 2 kg, and inherits extremely low impact properties, such as an effective mass of less than 0.4 kg in non near-singular configurations, enabling safe operation even in case of high velocities. The results are validated in simulation and experiments.

I. INTRODUCTION

Robots in human environments can pose a safety risk that is not easy to cope with. Especially during physical human-robot interaction collisions can not always be avoided or are even part of the process. Therefore, a lot of research has been and is being conducted on safe robot arms for increased collision safety needed for these applications.

Lightweight design and active compliance combined with collision detection and reaction schemes [1] can increase safety for robots. Because the bandwidth of actively controlled compliance is limited to the bandwidth of the sensors, actuators, and controller frequency, more effort is necessary for applications with high velocity and safety requirements.

Mechanisms with mechanical gravity compensation can improve fail-safe properties [2], but are mechanically complex. Aside from lightweight design safety can be improved by decoupling the link from the actuator. This can be achieved by using mechanisms that behave compliant in case of collisions [3] or with passive drivetrain compliance [4]–[6]. Another concept uses two combined actuators with complementing bandwidth features and connects the heavier and stronger actuator with a series elastic cable transmission to the joint [7]. Other concepts use cable transmission [8] or light-weight actuators with inherent compliant properties [9]. Passive elasticity between motor and joint can store energy, which can be beneficial for some applications. But the energy stored in this intrinsic compliance can also be harmful. These systems also suffer from degradation of the position control.

Variable impedance by changing the stiffness of the elastic transmission with two motors can be used to regain control bandwidth with high impedance while benefitting from low

impedance during fast motions or in contact situations [10]. In contact situations, however, and in applications that benefit from energy storage, elasticity can increase stability and drastically reduce energy consumption [11], [12].

Many applications in service robotics require high velocities in strongly unstructured environments, where impacts and clamping can occur on a frequent basis when making extensive use of physical human-robot interaction. Using collision detection in these environments can be a serious problem, because a reaction to a collision in uncertain environments can be dangerous by itself.

Several approaches try to simultaneously achieve collision safety and force/position tracking accuracy. In most cases, however, these approaches are not fail-safe, often too heavy, and have to be operated at reduced speed near humans. Also, clamping is a concern, especially with joints with brakes and high transmission ratio, causing high reflected damping, and with heavy links. Without collision detection, effects such as clamping in near-singular configurations can pose a big threat [13], even for low-inertia robots. As additionally sensor, hardware and software failures can occur, the use of low-power motors should be considered in order to reduce dangerous effects.

This paper presents the design of four degrees of freedom (DOF) BioRob robot arm (Fig. 1) targeted at service robotics applications featuring high intrinsic safety, low power consumption, high maximum joint velocities comparable to the human arm and low impedance for increased safety even for high-velocity clamping impacts. It is shown that the arm is both safe and suitable with respect to performance for applications with physical human-robot interaction.

This paper is organized as follows. Section II gives an outline of metrics for safety evaluation. Section III describes the robot arm design and Section IV discusses its safety properties for human-robot interaction applications. Experimental validation is given in Section V, along with quantitative safety properties of the BioRob arm. The paper concludes with a summary of the results and open issues to be addressed in future work.

II. SAFETY METRICS

For conventional industrial robots it makes sense to focus on the danger of severe injuries, for which the Head Injury Criterion (HIC) is a good measure. For lightweight service robots, other criteria for measuring the danger of lower severity injuries are needed. A thorough study by [13] examined criteria such as bone fracture forces and injury

The authors are with the Simulation, Optimization and Robotics Group, Department of Computer Science, Technische Universität Darmstadt, Germany [lens,stryk]@sim.tu-darmstadt.de

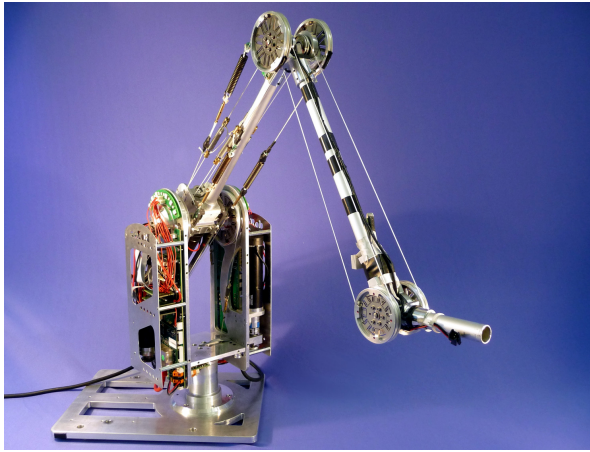


Fig. 1. BioRob-X4 (4 DOF) arm without gripper.

criteria vulnerable for specific areas of the body, such as chest compression.

Industrial safety standards, such as [14], have been conceived for industrial manipulators with the main goals of preventing bone fractures and laceration. For fast applications either a maximum dynamic power of 80 W or a maximum static force of 150 N are allowed.

A method to evaluate skin stress in blunt impact depending on the shape and material properties of the robotic arm was proposed in [15]. A detailed study of a realistic collision model of a robot arm with soft covering and human head with multi-layer structure for covering design to prevent soft-tissue injuries was presented in [16]. To evaluate the danger of contusions, a maximum impact energy density of 2.52 J/cm^2 and for lacerations, the skin tensile strength of $\sigma = 10^6 \text{ N/m}^2$ was used.

In contrast to safety, which can be defined as prevention of injury, pain is a very subjective measure. But nevertheless, it can be important for human-robot applications to also consider pain limits. Pain thresholds can be given as separate pressure limits for the static and dynamic case. The lowest Pressure Pain Thresholds (PPT's) reported in literature refer to the temporal areas of the head [17], [18], with maximum static pressure of $\sigma_{s,\max} = 150 \text{ kN/m}^2$ and maximum dynamic pressure of $\sigma_{c,\max} = 250 \text{ kN/m}^2$.

As was shown in [13], unconstrained collisions (depicted in Fig. 4) without clamping are not as dangerous as previously assumed with respect to serious injuries, even with heavy industrial robots. However, constrained impacts are pointed out as the most difficult and dangerous safety issue (see Fig. 4). For such impacts with sharp objects a collision detection and reaction scheme was presented that is capable of preventing injuries up to a certain velocity limit [?].

III. BIROB HARDWARE DESIGN & PROPERTIES

The BioRob-X4 robot arm, depicted in Fig. 1, consists of four joints that are elastically coupled by cables with built-in translational springs to the electrical motors. Important parameters of the arm comprise, aside from the Denavit Hartenberg (DH) parameters, the center of mass r_c , mass

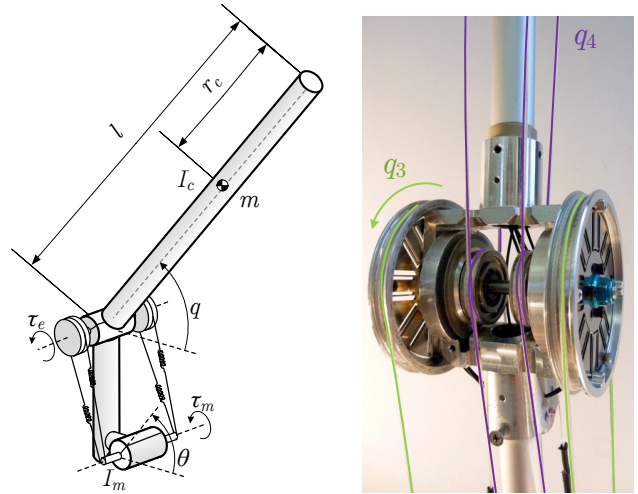


Fig. 2. BioRob arm joint actuation principle. Elastic tendon actuation of joints 1–3 (left). Elastic tendon actuation of joint 4 spanning two joints causing joint equilibrium position shifting (right).

m , transmission ratio z , rotor inertia I_r and joint stiffness k_e (cf. Table I). Two of the motors are located in the first link and two as a counterweight in the second link. Thus, most of the mass is located near the base and the center of mass of the second link r_{c2} is located at the axis of joint 2 (cf. DH parameter a_2). The joint actuation principle is illustrated in Fig. 2.

The joint equilibrium positions \hat{q} are defined by the current motor positions θ . The cable routing of joint q_4 with a pulley in joint 3 causes a shift α_{eq} of the equilibrium position \hat{q}_4 defined by current joint position q_3 and the radius $r_{d,3}$ of the deflection pulley in joint 3 and the radius r_4 of the pulley in joint 4 [6]:

$$\hat{q}(\theta, q) = \begin{pmatrix} \theta_1 \\ \theta_2 \\ \theta_3 \\ \theta_4 - \frac{r_{d,3}}{r_4} \cdot q_3 \end{pmatrix} = \theta - \alpha_{eq}(q) \quad (1)$$

By defining reflected motor and actuation parameters and variables by the combined gearbox und transmission ratio z , the dynamics model of elastic joint manipulators can be used [19]:

$$I_m \ddot{\theta} + D_m \dot{\theta} + \tau_e = \tau_m \quad (2)$$

$$M(q) \ddot{q} + C(q, \dot{q}) \dot{q} + D\dot{q} + g(q) = \tau_e \quad (3)$$

with output torque τ_e of the elastic tendon actuators depending on the current joint positions q and the joint equilibrium positions \hat{q} :

$$\tau_e = K_e \cdot (\hat{q}(\theta, q) - q) + D_e \cdot (\dot{\hat{q}}(\theta, \dot{q}) - \dot{q}) \quad (4)$$

Important parameters are listed in Table I. All actuator parameters are given with respect to the joint. For a detailed description of the kinematics and dynamics model we refer to [6].

The built-in translational springs in the cables decouple the links and motors, similar to the original series elastic actuator

TABLE I
IMPORTANT MODEL PARAMETERS OF THE BIO ROB-X4 ARM (WITH GRIPPER) WITH RESPECT TO THE JOINT SIDE.

Joint	1	2	3	4
DH (d, a, α)	$(0.276, 0, \frac{\pi}{2})$	$(0, 0.307, 0)$	$(0, 0.310, 0)$	$(0, 0.17, 0)$
r_c [m]	$(0, -0.138, 0)$	$(-0.297, 0, 0)$	$(-0.155, 0, 0)$	$(-0.070, 0, 0)$
m [kg]	2.350	1.530	0.160	0.204
I_z [kgm ²]	0.0449	0.0122	0.0051	0.0025
I_m [kgm ²]	0.0185	0.0218	0.0075	0.0029
k_e [Nm/rad]	100	80	35	6
$\tau_{m,max}$ [Nm]	9.5	10.4	6.1	6.2
z [-]	73.6	80.0	47.0	52.8
α_{eq} [-]	$(0, 0, 0, 0)$	$(0, 0, 0, 0)$	$(0, 0, 0, 0)$	$(0, 0, -0.5, 0)$

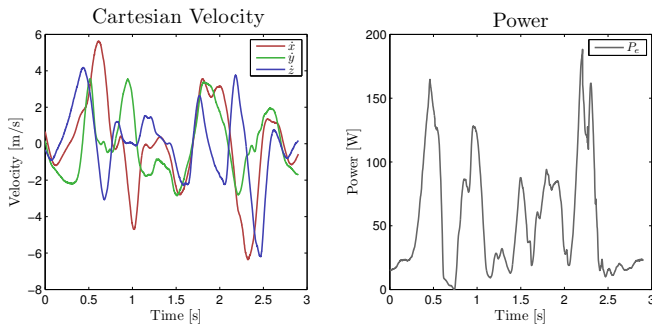


Fig. 3. Cartesian velocities and electrical power consumption of a fast trajectory.

[4], and enable additionally manual pretension, with the potential to decrease backlash effects. The low-pass filtering effect on force peaks protects the transmission system and geared motors from shocks (see Section IV), as elaborated in many previous works.

The joint elasticity k_e and the absence of joint brakes also enable high backdrivability, a property that is lost when using gearboxes with high reduction ratios or low efficiency, and increase the stability in contact situations. The design of BioRob-X4 allows the use of smaller motors with lower transmission ratio z and rotor inertia I_r , eventually leading to low reflected rotor inertia. As can be seen from Table I, the design of the robot arms leads to a link inertia lower than the reflected motor inertia in links 2–4. Decoupling of motor and joint inertia is therefore very important and effective for this design.

Without payload the robot arm is capable of performing extremely fast motions due to its low inertia. Fig. 3 displays such a trajectory with Cartesian velocities as high as 6.88 m/s with very low mean power consumption of 54 W for these high velocities. As can be seen, the dynamic peak power of the robot arm can easily exceed the 80 W limit for fast motions. With regard to the industrial safety norm, a maximum static force of 150 N is therefore important, which is evaluated in Section V-B.

The design leads to a very low overall weight of the robot arm of 4 kg (including power electronics), while still being able to carry an end-effector load of 2 kg without exceeding the maximum torques.

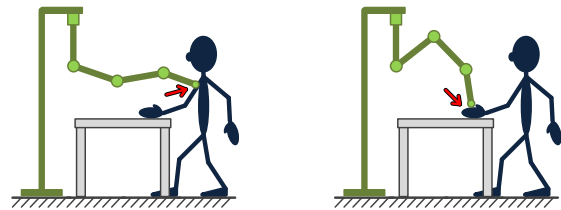


Fig. 4. Unconstrained (left) and constrained (right) collision (cf. [13]) in a typical pick-and-place scenario of a lightweight, mobile robot arm. For the worst-case analysis in this paper, a fixed robot base is assumed. The robot arm can therefore also be mounted in a suspended configuration [20].

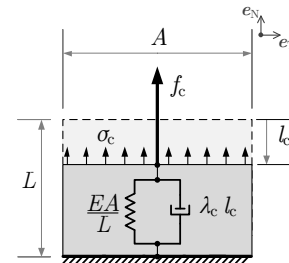


Fig. 5. Collision model used in simulation [21].

IV. COLLISION AND CLAMPING SAFETY

In this section, an upper limit estimation for occurring contact forces depending on joint configuration and velocity is calculated. It is assumed that all kinetic energy of the robot arm is dissipated or transformed into potential energy of the elastic contact during the collision by deformation of the contact area. This is true for clamping situations and collisions with objects with a considerably higher mass compared to the effective mass of the robot at the contact point.

A. Dynamic Impact

Methods for estimation of contact force and stress were presented in [15] and [16]. We extend these methods for robotic arms with joint elasticity by considering the potential energy stored in the springs. In addition, the static clamping case is considered.

The effective mass, or reflected inertia, at the end effector is given by the operational space inertia matrix Λ_c [22]

$$\Lambda_c(q) = (J(q) M(q) J(q)^T)^{-1}, \quad (5)$$

where J is the Jacobian and M the inertia matrix of the manipulator. The mass matrix M incorporates the additional mass of a load at the end effector, if present.

Assuming an elastic collision, the impact is modeled as a spring, where the kinetic energy of the robot arm is stored as potential energy. Regarding a constrained impact, it is assumed that during the impact all kinetic energy from the robot arm is transferred into potential energy of the elastic contact

$$\frac{1}{2} l_c^2 k_c = E_{kin} = \frac{1}{2} \mathbf{v}_c^T \Lambda_c \mathbf{v}_c, \quad (6)$$

with spatial velocity \mathbf{v}_c , collision stiffness k_c , and collision compression l_c .

When calculating the operational space inertia matrix for systems with $n < 6$ DOF, the Jacobian has to be reduced to contain only independent rows. Therefore, it is more convenient to calculate the kinetic energy in joint space:

$$l_c = \sqrt{\frac{\dot{\mathbf{q}}^\top \mathbf{M}(\mathbf{q}) \dot{\mathbf{q}}}{k_c}}, \quad (7)$$

with $\dot{\mathbf{q}}$ denoting the joint velocities.

By this means, it is possible to use the maximum spring force in the elastically deformed contact area to estimate an upper bound for the peak collision force:

$$f_c = k_c l_c = \sqrt{k_c \dot{\mathbf{q}}^\top \mathbf{M}(\mathbf{q}) \dot{\mathbf{q}}}. \quad (8)$$

By modeling the contact area and cushioning the robot as a layer of thickness L with elastic modulus E and contact surface A ,

$$f_c = \sqrt{\frac{EA}{L} \dot{\mathbf{q}}^\top \mathbf{M}(\mathbf{q}) \dot{\mathbf{q}}}, \quad (9)$$

the medium normal pressure σ_c on this contact surface A can be formulated, as described in [21], as:

$$\sigma_c = \frac{f_c}{A} = \sqrt{\frac{E}{AL} \dot{\mathbf{q}}^\top \mathbf{M}(\mathbf{q}) \dot{\mathbf{q}}}. \quad (10)$$

B. Static Clamping

The static clamping force can be derived by transforming the joint actuator torques $\boldsymbol{\tau}_m$ and gravitational torques $\boldsymbol{\tau}_g = -\mathbf{g}(\mathbf{q})$ to Cartesian space using the Jacobian pseudoinverse:

$$\mathbf{f}_s = (\mathbf{J}_v^\top(\mathbf{q}))^+ (\boldsymbol{\tau}_m - \mathbf{g}(\mathbf{q})). \quad (11)$$

The maximum normal stress produced by this force on the contact surface A can be given as:

$$\sigma_s = \frac{1}{A} \|(\mathbf{J}_v^\top(\mathbf{q}))^+ (\boldsymbol{\tau}_{m,\max} - \mathbf{g}(\mathbf{q}))\|. \quad (12)$$

In addition, almost all available robot arms use high reduction ratios, reflecting the motor friction with the transmission ratio z to the joints. This leads to hardly backdrivable systems. Furthermore, many systems activate joint brakes in case of a collision to compensate for the gravitational forces of the robot structure. However, this also makes it impossible to push the robot away from the collision. In such case, the upper bound of the static clamping forces drastically increases and can go up to the values of the dynamic clamping forces.

As pointed out in [23], quasi-static clamping can lead to extremely high contact forces. This is the case in near-singular positions, where the Jacobian \mathbf{J} becomes singular. For lightweight robot arms, this problem can be mitigated to a certain extent by the use of low-power motors, highly backdrivable joints, and soft cushioning, reducing the clamping stress σ_s . The only really safe solution, however, is to avoid near-singular configurations.

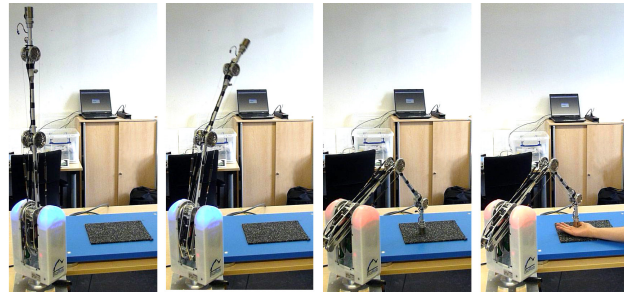


Fig. 6. Collision experiments without (frame 1–3) and with clamping a human hand (frame 4) using a force plate.

C. Potential Energy

In clamping situations, a high amount of potential energy can be stored in the springs:

$$E_{\text{pot,e}} = \frac{1}{2} (\hat{\mathbf{q}} - \mathbf{q})^\top \mathbf{K}_e (\hat{\mathbf{q}} - \mathbf{q}) \quad (13)$$

If this potential energy is suddenly released by breaking away from the collision, it can pose a danger.

V. SIMULATION AND EXPERIMENTAL RESULTS

To validate the presented approach, collisions were conducted in simulation and experiment with a typical trajectory of pick-and-place application where constrained clamping can occur (Fig. 4). The force measurement was performed with a force plate, as shown in Fig. 6. The desired end effector position of the robot arm was placed below the force plate, in order to generate a colliding trajectory with static clamping characteristics (Fig. 7). No collision detection and reaction strategy was activated.

The contact stiffness was determined by using estimated values for the contact area A , the layer thickness L and Young's Modulus E . Calibration measurements and comparison with the simulated contact model then yielded a refined value of $k_c = 50 \text{ kN/m}$, which was used in the simulation.

A. Dynamic Impact

As depicted in Fig. 7 and 8, the impact occurs at $t_c = 0.96 \text{ s}$. The joint velocity before the impact amounts to

$$\dot{\mathbf{q}}(t_c) = (0 \quad -1.3741 \quad -1.8019 \quad -0.9496)^\top \text{ rad/s} \quad (14)$$

According to (9), the kinetic energy of the robot structure at impact,

$$E_{\text{kin}}(t_c) = \frac{1}{2} \dot{\mathbf{q}}^\top \mathbf{M}(\mathbf{q}) \dot{\mathbf{q}} = 0.2826 \text{ J}, \quad (15)$$

yields an estimate for the maximum contact area compression l_c and impact force peak f_c :

$$f_c = \sqrt{2k_c E_{\text{kin}}} = 168.1 \text{ N}. \quad (16)$$

This calculated value for the impact force peak matches the results of the simulation and experimental measurements, $f_{c,\text{real}} = 178.5 \text{ N}$ (cf. Fig. 9), quite well. The collision occurred with $v = 1.23 \text{ m/s}$ and a duration of approximately 7 ms for the first impact peak.

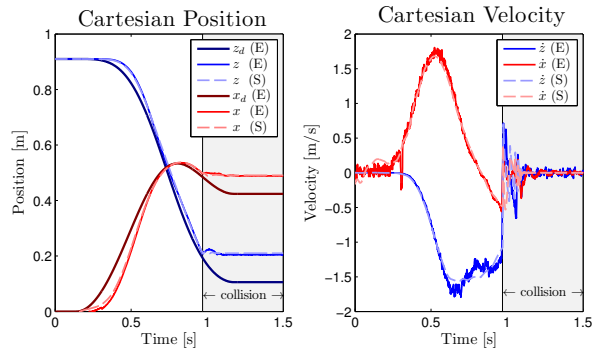


Fig. 7. Cartesian trajectory comparison of collision simulation (S) and experiment (E) with contact at $z_c = 0.205$ m and $t_c = 0.96$ s.

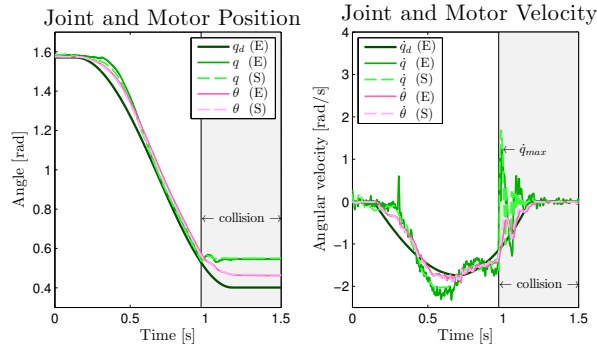


Fig. 8. Joint q and motor θ trajectory of joint 2 in collision simulation (S) and experiment (E). On the right, the joint velocity drop caused by the impact is marked with \dot{q}_{max} .

The effective masses of the robot arm at time of collision are $\Lambda_{c,zz} = 0.365$ kg in impact direction and $\Lambda_{c,xx} = 0.409$ kg in the frictional plane.

These values are at least one magnitude lower than the properties of comparable robot arms where the motors are directly located in the joints.

As can be seen in Fig. 10, the collision does not cause motor torque peaks. This can also be recognized in Fig. 8. There is no peak in the motor velocity. The motor is decelerated slowly, in contrast to the abrupt change in the joint velocity. The joint velocity peak after the collision is marked in the plot with \dot{q}_{max} .

B. Static Clamping

As depicted in Fig. 10, no collision detection is active. After the impact, beginning at $t_s = 1.5$ s, the robot arm pushes with constant motor torques τ_m and gravitational torques $-g(q)$ caused by the robot structure. The combined effect of the actuator and gravitational torques leads to a static clamping force of

$$\mathbf{f}_s = (\mathbf{J}_v^T)^+ \cdot (\boldsymbol{\tau}_m - \mathbf{g}) = -(2.386 \quad 0 \quad 16.860)^T. \quad (17)$$

For comparison, the real values from the experiments and simulation amount to:

$$\mathbf{f}_s = (2.000 \quad 0 \quad 16.975)^T. \quad (18)$$

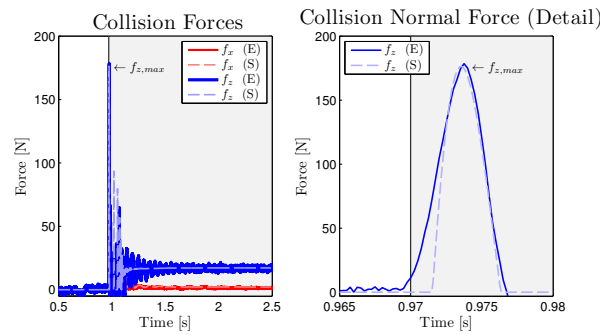


Fig. 9. Impact and static clamping forces in simulation (S) and experiment (E). A close-up of the first impact peak is displayed on the right, showing a peak width of 7 ms.

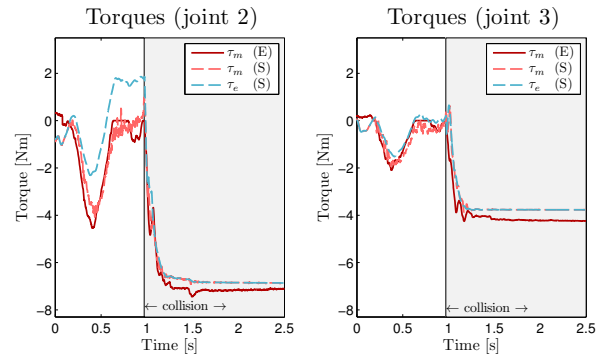


Fig. 10. Torques of joint 2 and 3 in collision simulation (S) and experiment (E). In contrast to the motor torque τ_m , the joint torque produced by the series elastic elements τ_e can not be directly measured during the experiment.

More of interest for safety evaluation, however, is the maximum clamping force that the actuators and robot arm weight can produce:

$$\mathbf{f}_{s,max} = (\mathbf{J}_v^T)^+ \cdot (\boldsymbol{\tau}_{m,max} - \mathbf{g}), \quad (19)$$

yielding

$$f_{s,max} = 24.7 \text{ N} \quad (20)$$

in this configuration.

Another very important measure is the stored potential energy in the springs:

$$E_{pot,springs} = \frac{1}{2} (\hat{\mathbf{q}} - \mathbf{q})^T \mathbf{K}_e (\hat{\mathbf{q}} - \mathbf{q}) = 2.06 \text{ J} \quad (21)$$

If released, this stored energy could, neglecting dissipative effects and assuming full conversion of potential to kinetic energy, produce a worst case impact force of

$$f_{c,pot} = \sqrt{2 \cdot k_c \cdot E_{pot,springs}} = 453 \text{ N}. \quad (22)$$

C. Resulting Pressure

The corresponding pressures can be derived from the impact forces:

$$\text{impact pressure: } \sigma_c = \frac{f_c}{A} = 319.5 \text{ kN/m}^2, \quad (23)$$

$$\text{clamping pressure: } \sigma_s = \frac{f_s}{A} = 28.5 \text{ kN/m}^2. \quad (24)$$

VI. DISCUSSION

The impact force and pressure is highly dependent on the contact area and stiffness. Therefore, covering design is important [16].

For the safety evaluation of the robot arm with series elastic tendon actuation we assumed only a small minimum contact area A and high collision stiffness k_e . Even with these parameters the impact pressure and impact energy are far below the safety limits. The maximum static clamping pressure of 25N is also far below the requirements of the industrial safety norm and of the defined safety limits in literature.

The energy stored into the springs in a clamping situation can be dangerous, if suddenly released. Therefore, a collision detection method is needed to make the motors compliant in such a case. Because of the non-self-locking motors in the proposed robot arm design, the energy stored in the springs is then transferred to the motors, where it dissipates. This is an advantage over the designs with non-backdrivable motors. These, on the other hand, can store energy in the springs more efficiently.

The maximum amount of potential energy $E_{\text{pot,springs}} = 2.06 \text{ J}$ that could be stored in the springs during clamping was almost one magnitude higher than the kinetic impact energy. It is therefore important to observe the amount of potential energy stored in the springs during operation.

VII. CONCLUSION

In this paper, the design and properties of a tendon-driven elastic joint robot arm for service robotics applications in unstructured environments with high velocity and safety requirements have been presented. The manipulator design allows to drastically reduce the total effective mass to less than 0.5 kg, while still maintaining the capability of manipulating loads up to 2 kg.

In addition, a safety evaluation method was proposed taking the potential energy stored in the springs into account. The presented method can be used to perform an on-line evaluation of the current safety state of the robot arm.

As minor obvious limitations, the proposed method is not capable of predicting an upper limit of the collision force or pressure for collisions with moving objects and manipulation of sharp objects. In these extreme cases only additional pre-contact safety may prove helpful.

ACKNOWLEDGMENT

This work has been supported by the German Federal Ministry of Education and Research BMBF under grant 01 RB 0908 A. The authors would like to thank Katayon Radkhah, Jürgen Kunz and Jérôme Kirchhoff for valuable discussion and comments and for the assistance with the experiments and the identification of the robot arm parameters.

REFERENCES

[1] S. Haddadin, A. Albu-Schäffer, A. De Luca, and G. Hirzinger, "Collision detection and reaction: A contribution to safe physical human-robot interaction," in *Proc. IEEE/RSJ Int. Conf. Intelligent Robots and Systems*, 2008, pp. 3356–3363.

[2] M. Vermeulen and M. Wisse, "Intrinsically safe robot arm: Adjustable static balancing and low power actuation," *Int. J. Social Robotics*, vol. 2, pp. 275–288, 2010.

[3] J.-J. Park, Y.-J. Lee, J.-B. Song, and H.-S. Kim, "Safe joint mechanism based on nonlinear stiffness for safe human-robot collision," in *Proc. IEEE Int. Conf. Robotics and Automation*, may 2008, pp. 2177–2182.

[4] G. Pratt and M. Williamson, "Series elastic actuators," *Proc. IEEE/RSJ Int. Conf. Intelligent Robots and Systems*, vol. 1, p. 399, 1995.

[5] T. Morita, H. Iwata, and S. Sugano, "Development of human symbiotic robot: Wendy," in *Proc. IEEE Int. Conf. Robotics and Automation*, vol. 4, 1999, pp. 3183–3188.

[6] T. Lens, J. Kunz, and O. von Stryk, "Dynamic modeling of the 4 DoF BioRob series elastic robot arm for simulation and control," in *Simulation, Modeling, and Programming for Autonomous Robots*, ser. Lecture Notes in Artificial Intelligence. Springer, 2010, pp. 411–422.

[7] M. Zinn, O. Khatib, B. Roth, and J. Salisbury, "Playing it safe [human-friendly robots]," *IEEE Robot. Autom. Mag.*, vol. 11, no. 2, pp. 12–21, 2004.

[8] B. Rooks, "The harmonious robot," *Industrial Robot: Int. J.*, vol. 33, pp. 125–130, 2006.

[9] A. Bicchi and G. Tonietti, "Fast and "soft-arm" tactics," *IEEE Robot. Autom. Mag.*, vol. 11, no. 2, pp. 22–33, 2004.

[10] R. Van Ham, T. Sugar, B. Vanderborght, K. Hollander, and D. Lefeber, "Compliant actuator designs," *IEEE Robot. Autom. Mag.*, vol. 16, no. 3, pp. 81–94, 2009.

[11] B. Vanderborght, B. Verrelst, R. Van Ham, M. Van Damme, D. Lefeber, B. M. Y. Duran, and P. Beyl, "Exploiting natural dynamics to reduce energy consumption by controlling the compliance of soft actuators," *Int. J. Robotics Research*, vol. 25, no. 4, pp. 343–358, 2006.

[12] S. Wolf and G. Hirzinger, "A new variable stiffness design: Matching requirements of the next robot generation," in *Proc. IEEE Int. Conf. Robotics and Automation*, 2008, pp. 1741–1746.

[13] S. Haddadin, A. Albu-Schäffer, and G. Hirzinger, "Requirements for safe robots: Measurements, analysis and new insights," *Int. J. Robotics Research*, vol. 28, no. 11-12, pp. 1507–1527, 2009.

[14] *ISO 10218-1:2009, Robots for industrial environments - Safety requirements - Part 1: Robot*, Std., 2009.

[15] M. Wassink and S. Stramigioli, "Towards a novel safety norm for domestic robotics," in *Proc. IEEE/RSJ Int. Conf. Intelligent Robots and Systems*, 2007, pp. 3354–3359.

[16] J. Park, S. Haddadin, J. Song, and A. Albu-Schäffer, "Designing optimally safe robot surface properties for minimizing the stress characteristics of human-robot collisions," in *Proc. IEEE Int. Conf. Robotics and Automation*, 2011, pp. 5413–5420.

[17] H. Buchanan and J. Midgley, "Evaluation of pain threshold using a simple pressure algometer," *Clin. Rheumat.*, vol. 6(4), pp. 510–517, 1987.

[18] K. Jensen, H. Andersen, J. Olesen, and U. Lindblom, "Pressure-pain threshold in human temporal region: evaluation of a new pressure algometer," *Pain*, vol. 25(3), pp. 313–323, 1986.

[19] S. Haddadin, A. Albu-Schäffer, and G. Hirzinger, "Soft-tissue injury in robotics," in *Proc. IEEE Int. Conf. Robotics and Automation*, 2010, pp. 3426–3433.

[20] M. W. Spong, "Modeling and control of elastic joint robots," *J. Dynamic Systems, Measurement, and Control*, vol. 109, no. 4, pp. 310–318, 1987.

[21] T. Lens, J. Kunz, C. Trommer, A. Karguth, and O. von Stryk, "Biorob-arm: A quickly deployable and intrinsically safe, light-weight robot arm for service robotics applications," in *Proc. 41st Int. Symp. Robotics / 6th German Conf. Robotics*, 2010.

[22] T. Lens, K. Radkhah, and O. von Stryk, "Simulation of dynamics and realistic contact forces for manipulators and legged robots with high joint elasticity," in *Proc. 15th Int. Conf. Advanced Robotics*, 2011, pp. 34–41.

[23] O. Khatib, "A unified approach for motion and force control of robot manipulators: The operational space formulation," *IEEE J. Robot. Autom.*, vol. 3, no. 1, pp. 43–53, 1987.

[24] S. Haddadin, A. Albu-Schäffer, M. Frommberger, and G. Hirzinger, "The role of the robot mass and velocity in physical human-robot interaction - part ii: Constrained blunt impacts," in *Proc. IEEE Int. Conf. Robotics and Automation*, 2008, pp. 1339–1345.